Research Article

# A genetically engineered oncolytic adenovirus decoys and lethally traps quiescent cancer stem-like cells in S/$G_2$/M phases

Shuya Yano[1], Hiroshi Tazawa[2], Yuuri Hashimoto[1], Yasuhiro Shirakawa[1], Shinji Kuroda[1], Masahiko Nishizaki[1], Hiroyuki Kishimoto[1], Futoshi Uno[1], Takeshi Nagasaka[1], Yasuo Urata[3], Shunsuke Kagawa[1], Robert M. Hoffman[4, 5], and Toshiyoshi Fujiwara[1]

**Author's Affiliations**

[1]Department of Gastroenterological Surgery, Okayama University Graduate School of Medicine, Dentistry and Pharmaceutical Sciences, Okayama, 700-8558, Japan; [2]Center for innovative clinical medicine, Okayama University Hospital, Okayama, 700-8558, Japan; [3]Oncolys BioPharma, Inc., Tokyo, 106-0032, Japan; [4]Department of Surgery, University of California San Diego, CA, 92103-8220; [5]AntiCancer, Inc., San Diego, CA, 92111.

**Corresponding Author:** Toshiyoshi Fujiwara, Department of Gastroenterological Surgery, Okayama University Graduate School of Medicine, Dentistry, and Pharmaceutical Sciences, 2-5-1 Shikata-cho, Kita-ku, Okayama 700-8558, Japan.

Phone: 81-86-235-7255; Fax: 81-86-221-8775; E-mail: toshi_f@md.okayama-u.ac.jp.

**Footnotes:**

**Abbreviations:** CS-like, cancer stem-like; LSC, leukemia stem cell; FUCCI, fluorescent ubiquitination cell cycle indicator; hTERT, human telomerase reverse transcriptase; Ad5, wild-type adenovirus type 5; MOI, multiplicity of infection; EGF, epidermal growth factor; PFU, plaque forming unit; PBGD, porphobilinogen deaminase; GAPDH, glyceraldehydes-3-phosphate dehydrogenase.

**Running title:** Elimination of quiescent cancer stem-like cells by adenovirus.

**Key words:** gastric cancer stem-like cell; quiescent/dormant; cell cycle; oncolytic virus.

**Manuscript information:** 28 text pages and 6 figures.

## Abstract

**Purpose:** Since chemo-radiotherapy selectively targets proliferating cancer cells, quiescent cancer stem-like (CS-like) cells are resistant. Mobilization of cell cycle in quiescent leukemia stem cells sensitizes them to cell death signals. However, it is unclear that mobilization of cell cycle can eliminate quiescent CS-like cells in solid cancers. Thus, we explored the use of a genetically engineered telomerase-specific oncolytic adenovirus, OBP-301 to mobilize the cell cycle and kill quiescent CS-like cells.

**Experimental design:** We established CD133$^{+}$ CS-like cells from human gastric cancer MKN45 and MKN7 cells. We investigated the efficacy of OBP-301 against quiescent CS-like cells. We visualized the treatment dynamics that OBP-301 killed quiescent CS-like cells in dormant tumor spheres and xenografts using fluorescent ubiquitination cell cycle indicator (FUCCI).

**Results:** CD133$^{+}$ gastric cancer cells had stemness properties. OBP-301 efficiently killed CD133$^{+}$ CS-like cells resistant to chemo-radiotherapy. OBP-301 induced cell cycle mobilization from $G_0/G_1$ to $S/G_2/M$ phase and subsequent cell death in quiescent CD133$^{+}$ CS-like cells by mobilizing cell-cycle related proteins. FUCCI enabled visualization of quiescent CD133$^{+}$ CS-like cells and proliferating CD133$^{-}$ non CS-like cells. Three-dimensional visualization of the cell cycle behavior in tumor spheres showed that CD133$^{+}$ CS-like cells maintained stemness by remaining in $G_0/G_1$ phase. We demonstrated that OBP-301 mobilized quiescent CS-like cells in tumor spheres and xenografts into $S/G_2/M$ phases where they lost viability and CS-like cell property, and became chemosensitive.

**Conclusion:** Oncolytic adenoviral infection is an effective mechanism of cancer cell killing in solid cancer and can be a new therapeutic paradigm to eliminate quiescent CS-like cells.

## Translational Relevance

Current chemotherapy and radiotherapy target proliferating cancer cells, while having little effect on dormant cancer cells. Cancer stem-like (CS-like) cells can maintain a quiescent or dormant state, which contributes largely to their resistance to conventional therapies. Recently, several therapeutic strategies have targeted inhibition of quiescent state in leukemia stem cells. However, it is still unclear whether CS-like cells in solid tumors can also be eliminated by inhibition of their dormant state. Here, we show that a telomerase-specific adenovirus, OBP-301, mobilizes quiescent CS-like cells to cycle and lethally traps them into S-phase. Moreover, we demonstrated a spatiotemporal treatment dynamics that OBP-301 decoyed quiescent CS-like cells in tumor spheres and xenografts into S-phase trap where they lost viability and CS-like cell property and become chemosensitive. Thus, our data provides that cell-cycle mobilization and S/$G_2$/M-phase-trapping induced by adenoviral infection is an effective mechanism of cancer cell killing of CS-like cells in solid cancers.

## Introduction

Current cytotoxic chemo-radiotherapy selectively targets proliferating cancer cells. Quiescent or dormant cancer cells in contrast are often drug resistant and are a major impediment to cancer therapy (1, 2). Cancer stem-like (CS-like) cells or tumor-initiating cells (3-5) maintain a quiescent or dormant state, which appears to contribute to their resistance to conventional therapies (6-8). Recently, several therapeutic strategies have targeted inhibition of the CS-like cell quiescent state. For example, treatment with arsenic trioxide enhanced the sensitivity of Leukemia stem cells (LSCs) to cytosine arabinoside through inhibition of LCS quiescence (9). Acute myeloid leukemia stem cells can be induced to enter the cell cycle and apoptosis by treatment with granulocyte colony-stimulating factor (10). However, it is still unclear whether CS-like cells in solid tumors can also be eliminated by inducing them to cycle.

Viruses can infect target cells, multiply, cause cell death and release viral particles. These features enable the use of viruses as anticancer agents that induce specific tumor lysis (11, 12). Adenoviral E1A, in particular, has been shown to exert tumor suppressive functions, including enhancement of chemoradiotherapy-induced apoptosis via inhibition of the cellular DNA repair machinery (13), and inhibition of cell proliferation via suppression of epidermal growth factor receptor (EGFR) (14) and HER2 (15). It has been recently reported that an oncolytic adenovirus efficiently eradicates CS-like cells as well as non-CS-like cells in brain tumors, breast cancer, and esophageal cancer (16-18).

In the present study, we isolated $CD133^+$ subpopulations from radioresistant cells in human gastric cancer cell lines and characterized them as CS-like cells. By using multicolor cell cycle imaging that color-codes the quiescent CS-like cells and proliferating non-CS-like cells, we demonstrated the treatment dynamics that a genetically engineered telomerase-specific oncolytic adenovirus, OBP-301 (19, 20) eradicates dormant $CD133^+$ CS-like cells via cell-cycle mobilization both in tumor spheres and in subcutaneous tumors.

## Materials and Methods

**Cell lines and radiation treatment.**

The human gastric cancer cell lines MKN45 and MKN7 were maintained according to the vendor's specifications (21). Radioresistant MKN45 and MKN7 cells were established by administration of radiation treatments using an X-ray generator (MBR-1505R; Hitachi Medical Co.)

**Recombinant adenoviruses.**

The recombinant tumor-specific, replication-selective adenovirus vector OBP-301 (Telomelysin), in which the promoter element of the human telomerase reverse transcriptase (hTERT) gene drives the expression of E1A and E1B genes linked to an internal ribosome entry site, was previously constructed and characterized (19, 22).

**Isolation of $CD133^+$ and $CD133^-$ cells by flow cytometry.**

After incubated with an anti-CD133/2(293C)-Allophycocyanin antibody (Miltenyi Biotec), $CD133^+$ cells were sorted by flow cytometry using FACSAria flow cytometer (Becton Dickinson). $CD133^+$ and $CD133^-$ cells were separated by flow cytometry just before each experiment to ensure that the purity of the $CD133^+$ population was greater than 70%, and the purity of $CD133^-$ cells was above 99%.

**Cell viability assay.**

CD133$^{+}$ and CD133$^{-}$ cells ($5 \times 10^{2}$ cells/well) in 96-well plates were treated with OBP-301, cisplatin or radiation at the indicated doses. Cell viability was determined on day 5 after treatment using the Cell Proliferation Kit II (Roche Molecular) according to the manufacturer's protocol.

**Establishment of MKN45 cells stably transfected with FUCCI vector plasmids.**

FUCCI (Fluorescent ubiquitination-based cell cycle indicator) system (23) was used to visualize the cell cycle phases. Plasmids expressing mKO2-hCdt1 (green fluorescence protein) or mAG-hGem (orange fluorescence protein) were obtained from the Medical & Biological Laboratory. Plasmids expressing mKO2-hCdt1 or mAG-hGem were transfected into radioresistant MKN45 cells using Lipofectamine LTX (Invitrogen).

**Western blot analysis.**

The primary antibodies used were: mouse anti-CD133/1(W6B3C) monoclonal antibody (mAb) (Miltenyi Biotec), rabbit anti-E2F1 polyclonal antibody (pAb) (Santa Cruz Biotechnology), mouse anti-Ad5 E1A mAb (BD Pharmingen), mouse anti-c-Myc pAb, rabbit anti-phospho-Akt mAb, rabbit anti-Akt mAb, mouse anti-p27 mAb (all three from Cell Signaling Technology), mouse anti-p53 mAb, mouse anti-p21 mAb (both from CALBIOCHEM Merck4 Biosciences), and mouse anti-β-actin mAb (Sigma-Aldrich). Immunoreactive bands on the blots were visualized using enhanced chemiluminescence substrates (ECL Plus; GE Healthcare).

**Subcutaneous MKN45 tumor xenograft model.**

To evaluate a tumorigenicity of $CD133^+$ and $CD133^-$ cells, purified $CD133^+$ and $CD133^-$ cells in radioresistant MKN45 were inoculated at a density of $1 \times 10^5$ cells/site on the right and left sides, respectively, of the flank of 5-week-old female NOD/SCID mice (Charles River Laboratories) or athymic nude mice (Charles River Laboratories). To evaluate the *in vivo* antitumor effect of OBP-301, cisplatin or radiation, the radioresistant MKN45 cells were inoculated at a density of $5 \times 10^6$ cells/site into the flank of 5-week-old female athymic nude mice. OBP-301 ($1 \times 10^8$ plaque forming units (PFU)) was injected into the tumors. Cisplatin (4 mg/body weight (kg)) was intraperitoneally injected and ionizing radiation (2 Gy) was performed into tumors after protection of normal tissues. Mice were treated every 3 days for a total of three treatments.

**Imaging of MKN45 cells expressing cell cycle-dependent fluorescent proteins.**

Time-lapse images of FUCCI expressing $CD133^+$ and $CD133^-$ radioresistant MKN45 cells were acquired using a confocal laser scanning microscope (FV10i; Olympus). Cross-sections of FUCCI-expressing tumors were imaged using confocal laser scanning microscope (FV-1000; Olympus).

**Treatment of subcutaneous FUCCI-expressing MKN45 tumors.**

To evaluate the *in vivo* antitumor efficacy of OBP-301, cisplatin, paclitaxel or combination, the FUCCI-expressing MKN45 cells were inoculated at a density of $5 \times 10^6$ cells/site into the flank of 5-week-old female athymic nude mice (Charles River Laboratories). OBP-301 ($1 \times 10^8$ PFU/tumor) was injected into the tumors. Cisplatin (4 mg/kg) and paclitaxel (5 mg/kg) were injected intraperitoneally. Mice were treated every 3 days for a total of three to five treatments.

.

**Statistical analysis.**

Data are shown as means ± SD. For comparison between two groups, significant differences were determined using Student's t-test. For comparison of more than two groups, statistical significance was determined with a one-way analysis of variance (ANOVA) followed by a Bonferroni multiple group comparison test. P values of < 0.05 were considered significant.

## Results

**$CD133^+$ cells in human gastric cancer cells are cancer stem-like.**

CS-like cells are more resistant to radiotherapy than non-CS-like cells (24-26). To enrich CS-like subpopulations, we established radioresistant MKN45 and MKN7 human gastric cancer cells. Radioresistant MKN45 and MKN7 cells significantly had a higher percentage of $CD133^+$ cells than parental cells (Fig. 1A and Supplementary Fig. S1A). We hypothesized that CD133 in gastric cancer would identify cancer cells with stem-like properties, such as asymmetric cell division, *in vitro* proliferation, dormancy, sphere formation, and *in vivo* tumorigenicity (5, 6). To investigate the asymmetric division of $CD133^+$ cells, we determined if $CD133^+$ cells produce both $CD133^+$ and $CD133^-$ cells. $CD133^+$ cells generated both $CD133^+$ and $CD133^-$ cells, whereas $CD133^-$ cells could not produce $CD133^+$ cells (Supplementary Fig. S2). We compared *in vitro* proliferation of $CD133^+$ and $CD133^-$ cells. $CD133^+$ cells produced larger colonies than $CD133^-$ cells. (Fig. 1B and Supplementary Fig. S3). $CD133^+$ cells made significantly much more tumor spheres than $CD133^-$ cells (Fig. 1B). $CD133^+$ cells produced tumors in immunodeficient nude mice and NOD/SCID mice, whereas $CD133^-$ cells did not generate any tumor in either nude on NOD/SCID mice (Supplementary Fig. S4 and Fig. 1B). Furthermore, $CD133^+$ cells in radioresistant MKN45 and MKN7 cells were significantly more resistant to 5-fluorouracil, cisplatin, paclitaxel, and radiation than $CD133^-$ cells (Fig. 1C and Supplementary Fig. S1B). These data indicate that $CD133^+$ cells are CS-like.

**Quiescent $CD133^+$ CS-like cells and cycling $CD133^-$ non-CS-like cells are independently visualized by fluorescent cell cycle indicator technology**

Sakaue-Sawano et al. have reported that the cell cycle state in viable cells can be visualized using the fluorescent ubiquitination-based cell cycle indicator (FUCCI) system (23). We established FUCCI-expressing $CD133^+$ or $CD133^-$ radioresistant MKN45 cells, in which cell nucleus at $G_0$/ $G_1$, S, or $G_2$/M phase exhibit red, yellow, or green fluorescence, respectively. We compared the cell cycle phase of FUCCI-expressing $CD133^+$ or $CD133^-$ cells. Time-lapse imaging showed that most of $CD133^+$ cells were quiescent in $G_0$/ $G_1$ phase with red fluorescent nuclei compared with $CD133^-$ cells (Fig. 1D). Similar results were also observed in flow cytometry analysis of cell cycle (Supplementary Fig. S5A and S5B). $CD133^+$ cells had similar proliferation rates as $CD133^-$ cells until 3 days after seeding. $CD133^+$ cells showed lower proliferation rate than $CD133^-$ cells 5 days after seeding (Fig. 1D). This result was consistent with the cell cycle status of $CD133^+$ cells which had an increased percentage of cells in $G_0$/ $G_1$ phase. Moreover, we examined the cell cycle-related protein (27) expression in $CD133^+$ and $CD133^-$ cells. $CD133^+$ cells showed higher expressions of p53, p21 and p27 proteins compared with $CD133^-$ cells (Supplementary Fig. S8), suggesting that these proteins are involved in the maintenance of quiescent CS-like cells.

**OBP-301 efficiently kills CS-like cells with reducing CS-like cell frequency via enhanced viral replication.**

To evaluate the efficacy of OBP-301 against CD133$^+$ CS-like cells, we treated CD133$^+$ and CD133$^-$ cells from radioresistant MKN45 and MKN7 cells with OBP-301. OBP-301 similarly killed CD133$^+$ and CD133$^-$ cells (Fig. 2A and Supplementary Fig. S1B). Next we investigated whether OBP-301 could decrease CS-like cell frequency. Flow cytometric analysis demonstrated OBP-301 significantly decreased the percentage of CD133$^+$ cells compared with cisplatin or radiation (Fig. 2A). Expression of *CD133* mRNA was closely associated with the population of CD133$^+$ cells (Supplementary Fig. S6). OBP-301 significantly suppressed the expression of CD133 mRNA compared with cisplatin and radiation (Supplementary Fig. S7). Western blot analysis also showed that cisplatin and radiation, but not OBP-301, increased three to fivefold CD133 expression in CD133$^+$ cells (Fig. 2D). Moreover, pre-treatment of CD133$^+$ cells with OBP-301, not cisplatin or radiation, significantly decreased the number of tumor spheres (Supplementary Fig. S13). These data indicated that OBP-301 kills both CD133$^+$ and CD133$^-$ cells with reducing CS-like cell frequency.

To further explore the efficacy of OBP-301 against CD133$^+$ CS-like cell, we assessed the relationship between hTERT activity and viral replication. OBP-301 contains the hTERT promoter, which allows it to tumor-specifically regulate the gene expression of E1A and E1B for viral replication (19). Quantitative reverse transcriptation-polymerase chain reaction (qRT-PCR) showed that CD133$^+$ cells had a significant, 3-fold higher expression of *hTERT* mRNA than CD133$^-$ cells (Fig. 2B), suggesting that CD133$^+$ CS-like cells have a higher activity of hTERT than CD133$^-$ cells. Next we compared the expression of *E1A* mRNA and E1A protein in CD133$^+$ cells and in CD133$^-$ cells. qRT-PCR showed that the expression of

*E1A* mRNA in CD133$^+$ cells was higher than that in CD133$^-$ cells (Fig. 2B). Western blotting analysis showed that the expression of E1A in CD133$^+$ cells was higher than that in CD133$^-$ cells (Fig. 2B). Furthermore we compared the copy number of the E1A gene, which is indicative of viral replication, in CD133$^+$ and CD133$^-$ cells after infection with OBP-301. As expected, the copy number of the E1A gene in CD133$^+$ cells was significantly higher than that in CD133$^-$ cells (Fig. 2B). These data indicate that OBP-301 is efficiently cytopathic for CD133$^+$ cells due to the enhanced viral replication.

**OBP-301 mobilizes and lethally traps quiescent CS-like cells into S-phase in monolayer culture.**

To examine whether OBP-301 could change the cell cycle phase of quiescent CD133$^+$ cells, we treated FUCCI-expressing CD133$^+$ cells with OBP-301. Time-lapse imaging showed that OBP-301 infection significantly decreased the percentage of CD133$^+$ cells in $G_0$/ $G_1$ phase, increased the percentage of CD133$^+$ cells in S phase, and killed them at S-phase (Fig. 2C and Supplementary Movie S1). Similar results were also observed in flow cytometry analysis of cell cycle (Supplementary Fig. S5C and S5D). These results suggest that OBP-301 induces cell cycle activation of quiescent CD133$^+$ cells from $G_0$/ $G_1$ phase to S phase and kills them. We next assessed the molecular mechanism by which OBP-301 induces mobilization of cell cycle in quiescent CS-like cells. OBP-301 increased the expression of E2F1, c-Myc and phospho-Akt proteins that function as cell cycle accelerators (27) and decreased the expression of p53, p21 and p27 proteins that function as cell cycle brakes (27) in quiescent CD133$^+$ cells (Fig. 2D). In contrast, cisplatin and radiation increased the expression of p53 and p21 proteins (Fig. 2D). We further examined whether adenoviral E1A altered the expression of these proteins in CD133$^+$ cells. E1A-expressing OBP-301 and Ad5, but not E1A-defficient dl312, similarly altered the expression of these proteins in CD133$^+$ cells (Supplementary Fig. S9). These results indicate that OBP-301 induces cell cycle progression through upregulation of E2F-related proteins and downregulation of p53-related and p27 proteins by enhanced adenoviral E1A in quiescent CS-like cells.

**Three-dimensional tumor spheres maintain CD133$^+$ subpopulation by keeping quiescent.**

Formation of tumor spheres under serum-free conditions is frequently used to maintain CS-like cell subpopulations (28). The addition of serum makes floating undifferentiated tumor spheres migrate from sphere to adherent cells and differentiate into adherent cells (29). Therefore, we hypothesized that tumor sphere maintained CS-like cell frequency due to be quiescent. CD133$^+$ cells at each cell cycle in three-dimensional culture gathered, formed tumor spheres, and became in $G_0/G_1$ phase (Fig. 3A). Tumor spheres from CD133$^+$ cells contained more quiescent cells than those from CD133$^-$ cells (Fig. 3B). Moreover, the established tumor spheres from CD133$^+$ cells in three-dimensional culture without serum remained quiescence (Fig. 3C). In contrast, the established tumor spheres, after adding serum, exited from quiescent state and began to cycle, divide and increase (Fig. 3C and Supplementary Movie S2). Flow cytometric analysis demonstrated that CD133$^+$ cells could be maintained in tumor spheres cultured in serum-free medium for 2 weeks, whereas the percentage of CD133$^+$ cells significantly decreased in CD133$^+$ cells cultured in monolayer cultures or in tumor spheres cultured in serum-containing medium (Fig. 3D). These data indicate that tumor sphere maintains CSC frequency keeping dormant.

**Real-time imaging spatiotemporally shows OBP-301 eliminates dormant tumor spheres**

**by cell-cycle mobilization and $S/G_2/M$-phase-trapping.**

To further evaluate OBP-301 induced cell-cycle mobilization and S-phase-trapping in dormant tumor sphere, we visualized the treatment dynamics of FUCCI-expressing tumor spheres with OBP-301 infection. Time-lapse imaging demonstrated OBP-301 infected quiescent $CD133^+$ cells at the periphery of the spheres and then induced S and $G_2/M$ phase entry, leading to the cellular death by viral replication (Fig. 4A). Moreover, as OBP-301 penetrated into the deeper layers, tumor spheres gradually shrunk after virus infection (Fig. 4A, 4C). In contrast, cisplatin and radiation did not affect the cell cycle phase or the size of tumor spheres (Figs. 4A, 4B, 4C and Supplementary Movie S3). Immunofluorescent staining of tumor spheres also confirmed that OBP-301 infection downregulated CD133, p53, and p21 expression, and upregulated E2F1 and phospho-Akt expression in tumor spheres (Fig. 4D). These results suggest that OBP-301 efficiently eradicates dormant tumor sphere resistant to conventional therapies by mobilizing them into an $S/G_2/M$-phase trap.

**OBP-301 efficiently kills dormant cancer stem-like cells in established human tumor xenografts by cell-cycle mobilization and $S/G_2/M$-phase-trapping thereby reducing cancer stem-like cell frequency.**

To further confirm whether OBP-301 efficiently reduced $CD133^+$ CS-like cell frequency within tumor tissues (Supplementary Figure S10A), we investigated the expression of *CD133* mRNA and CD133 positive ratio in subcutaneous tumors derived from radioresistant MKN45 cells after treatment of OBP-301, cisplatin or irradiation. Suppression of tumor growth by OBP-301 (Fig. 5A) was accompanied by a significant decrease in CD133 mRNA at 2 weeks after the final treatment (Fig. 5B). In contrast, although cisplatin and radiation also suppressed tumor growth to a similar extent as OBP-301 (Fig. 5A), cisplatin did not affect, and radiation significantly increased CD133 mRNA expression at 1 week after the final treatment (Fig. 5B). Immunohistochemistry of CD133-stained tumor sections also showed that OBP-301 reduced the frequency of $CD133^+$ cells, whereas cisplatin and irradiation increased compared with control (Fig. 5B).

Next we visualized the treatment dynamics in established FUCCI-expressing MKN45 tumor xenografts with or without OBP-301 infection (Supplementary Fig. S10B). FUCCI-expressing MKN45 tumors had the distribution of cancer cells in $G_0$/ $G_1$, S and $G_2$/M phases (Fig. 5A). As tumor grew bigger, cancer cells in $G_0$/ $G_1$ phase increased (Fig. 5C and 5D), indicating the existence of dormant cancer cells. After cisplatin or paclitaxel treatment, the tumor consisted mostly of red fluorescent cells (Fig. 5D), indicating that the cytotoxic agents killed only cycling cancer cells and had little effect on quiescent dormant cancer cells. These tumors re-grew with the quiescent cells re-entering the cell cycle 21 days after last treatment (Figs. 5D). In contrast, intratumor injection of OBP-301 mobilized the cancer cells into the S/$G_2$/M-phase trap in vivo, leading to elimination of tumor cells at S/$G_2$/M phases (Fig. 5D). These data indicate that OBP-301 could more efficiently kill quiescent CS-like cells in tumors by inducing cell-cycle progression.

**OBP-301 sensitizes quiescent cancer stem-like cells to chemotherapy by cell-cycle mobilization and S/$G_2$/M-phase-trapping.**

As we previously demonstrated that OBP-301 enhances the sensitivities to chemotherapeutic agents in various types of human cancer cells (30, 31), we further evaluated whether OBP-301 sensitizes quiescent $CD133^+$ CS-like cells to chemotherapy by inducing cell cycle progression and S/$G_2$/M-phase trapping. OBP-301 infection significantly enhanced the inhibitory effect of chemotherapy on the cell viability and tumor sphere formation of $CD133^+$ cells (Fig. 6A and Supplementary Fig. 13). Tumor spheres treated with chemotherapy and OBP-301 contained an increased percentage of tumor cells at $G_2$/M phases compared to OBP-301 alone (Fig. 6B). The combination of OBP-301 and chemotherapy (Supplementary Fig. S10C) significantly suppressed the tumor growth compared to chemotherapy or OBP-301 alone (Fig. 6C and Supplementary Fig. S14). Cross-sections of tumor tissues demonstrated that combination of chemotherapy and OBP-301 induced an increased percentage of tumor cells at $G_2$/M phases compared to OBP-301 alone (Fig. 6D). These results suggest that OBP-301 sensitizes the quiescent CS-like cells to chemotherapy-mediated $G_2$/M arrest by inducing cell cycle progression and S/$G_2$/M-phase-trapping.

## Discussion

Here we have described that a bioengineered telomerase-specific oncolytic adenovirus, OBP-301, efficiently kills $CD133^+$ CS-like cells that have higher telomerase activity through enhanced E1A-mediated cell-cycle mobilization and S-phase-trapping. By using FUCCI technology in combination with tumor-sphere culture, we visualized the virus penetration, the cell-cycle dynamics, and the subsequent elimination of quiescent CS-like cells in dormant tumor spheres (Supplementary Fig. S15A).

CS-like cells have been shown to be highly resistant to chemotherapeutic agents (32, 33) and ionizing radiation (24-26). As expected, $CD133^+$ human gastric cancer cells were more resistant to conventional therapies than $CD133^-$ cells; OBP-301, however, efficiently reduced the viability of $CD133^+$ cells as similar as $CD133^-$ cells. Moreover, we demonstrated that OBP-301 significantly reduced the stem cell properties of $CD133^+$ cells *in vitro* and *in* *vivo* compared with conventional chemoradiotherapy and further sensitized $CD133^+$ CS-like cells to chemotherapy. These findings indicate that OBP-301 is a promising anticancer therapy to eliminate CS-like cells more efficiently than conventional therapy in the clinical setting.

Recent studies have showed that p53 and $p21^{cip1/waf1}$ maintain the quiescent state in hematopoietic stem cells (34, 35). Moreover, $p27^{kip1}$ has been suggested to be involved in suppression of the transition from the $G_0$ phase to $G_1$/S phases (36, 37). CS-like cells maintain a more quiescent state than non-CS-like cells, which is associated with CS-like cell resistance to conventional therapies (9, 10). OBP-301 induced S and $G_2$/M phase entry and subsequent cell death in quiescent $CD133^+$ cells through upregulation of E2F1-related proteins and downregulation of p53-related and p27 proteins in an E1A-dependent manner. A recent report suggested that suppression of the p53-mediated $G_1$ checkpoint is required for E2F1-induced S phase entry (38). Furthermore, adenoviral E1A has been shown to suppress p53-mediated cell cycle arrest after DNA damage (39). Thus, OBP-301 can inhibit CS-like cells from maintaining quiescent state and enforce them into cell-cycling by not only upregulating E2F-related proteins, but also downregulating p53-related and p27 proteins (Supplementary Fig. S15B), leading to the sensitization to chemotherapy.

FUCCI (23) is a powerful tool to visualize the quiescent state in CS-like cells and the treatment dynamics of OBP-301 against quiescent CS-like cells. When tumor spheres were formed, $CD133^+$ cells maintained a quiescent state, which was defined by the red fluorescent nuclei expressed in $G_0$/ $G_1$ phases. In contrast, S and $G_2$/M phase entry induced by OBP-301 could be clearly visualized as yellow and green fluorescent nuclei, respectively. Our data indicate that three-dimensional cultures are extremely important for the maintenance of the quiescence of $CD133^+$ cells. FUCCI-based real-time imaging of the cell-cycle provides a platform for the screening of candidate therapeutic agents that modulate the quiescent state of drug-resistant CS-like cells.

In conclusion, we have clearly demonstrated that a genetically engineered oncolytic adenovirus, OBP-301, efficiently eradicates quiescent CS-like cells in solid tumors by cell-cycle mobilization and S/$G_2$/M-phase-trapping. A phase I clinical trial of intratumoral injection of OBP-301 in patients with advanced solid tumors recently completed and OBP-301 monotherapy was well tolerated by these patients (20). However, the adenoviral delivery to inaccessible primary and metastatic tumor tissues is a major obstacle for clinical translation of this treatment modality. In this study, the combination therapy of OBP-301 with chemotherapy was highly effective antitumor therapy to eliminate both CS-like and non-CS-like cells in a xenograft model. Future clinical trials of intratumoral injection of OBP-301 in combination with conventional antitumor therapy are suggested by the results of the present study.

## Disclosure of Potential Conflicts of Interest

Y. Urata is President & CEO of Oncolys BioPharma, Inc., the manufacturer of OBP-301 (Telomelysin). H. Tazawa and T. Fujiwara are consultants of Oncolys BioPharma, Inc.

## Author contributions

**Conception and design:** S. Yano, H. Tazawa, R. M. Hoffman, T. Fujiwara

**Development of methodology:** S. Yano, H. Tazawa, Y. Hashimoto, S. Kuroda, H. Kishimoto

**Acquisition of data (provided animals, provided facilities, etc):** S. Yano, H. Tazawa, Y. Hashimoto

**Analysis and interpretation of data (e.g., statistical analysis, biostatistics, computational analysis):** S. Yano, H. Tazawa, Y. Hashimoto, Nagasaka, S. Kagawa, T. Fujiwara

**Writing, review, and/or revision of manuscript:** S. Yano, H. Tazawa, R. M. Hoffman, T. Fujiwara

**Administrative, technical, or material support:** Y. Urata, R. M. Hoffman

**Study supervision:** H. Tazawa, Y. Shirakawa, M. Nishizaki, T. Nagasaka, S. Kagawa, R. M. Hoffman, T. Fujiwara

## Acknowledgments

We thank Yukinari Isomoto and Tomoko Sueishi for their technical support.

## Grant Support

This work was supported in part by grants from the Ministry of Education, Culture, Sports, Science, and Technology of Japan (to Toshiyoshi Fujiwara, No. 22390256) and by grants from the Ministry of Health, Labour, and Welfare of Japan (to Toshiyoshi Fujiwara, No. 10103827, No. 09156285).

## References


1. Goss PE, Chambers AF. Does tumour dormancy offer a therapeutic target? Nat Rev Cancer. 2010;10:871-7.
2. Aguirre-Ghiso JA. Models, mechanisms and clinical evidence for cancer dormancy. Nat Rev Cancer. 2007;7:834-46.
3. Reya T, Morrison SJ, Clarke MF, Weissman IL. Stem cells, cancer, and cancer stem cells. Nature. 2001;414:105-11.
4. Pardal R, Clarke MF, Morrison SJ. Applying the principles of stem-cell biology to cancer. Nat Rev Cancer. 2003;3:895-902.
5. Clarke MF, Dick JE, Dirks PB, Eaves CJ, Jamieson CH, Jones DL, et al. Cancer stem cells--perspectives on current status and future directions: AACR Workshop on cancer stem cells. Cancer Res. 2006;66:9339-44.
6. Visvader JE, Lindeman GJ. Cancer stem cells in solid tumours: accumulating evidence and unresolved questions. Nat Rev Cancer. 2008;8:755-68.
7. Trumpp A, Wiestler OD. Mechanisms of Disease: cancer stem cells--targeting the evil twin. Nat Clin Pract Oncol. 2008;5:337-47.
8. Zhou BB, Zhang H, Damelin M, Geles KG, Grindley JC, Dirks PB. Tumour-initiating cells: challenges and opportunities for anticancer drug discovery. Nat Rev Drug Discov. 2009;8:806-23.
9. Ito K, Bernardi R, Morotti A, Matsuoka S, Saglio G, Ikeda Y, et al. PML targeting eradicates quiescent leukaemia-initiating cells. Nature. 2008;453:1072-8.
10. Saito Y, Uchida N, Tanaka S, Suzuki N, Tomizawa-Murasawa M, Sone A, et al. Induction of cell cycle entry eliminates human leukemia stem cells in a mouse model of AML. Nat Biotechnol. 2010;28:275-80.
11. Alemany R, Balague C, Curiel DT. Replicative adenoviruses for cancer therapy. Nat Biotechnol. 2000;18:723-7.
12. Russell SJ, Peng KW, Bell JC. Oncolytic virotherapy. Nat Biotechnol. 2012;30:658-70.
13. Stracker TH, Carson CT, Weitzman MD. Adenovirus oncoproteins inactivate the Mre11-Rad50-NBS1 DNA repair complex. Nature. 2002;418:348-52.
14. Flinterman M, Gaken J, Farzaneh F, Tavassoli M. E1A-mediated suppression of EGFR expression and induction of apoptosis in head and neck squamous carcinoma cell lines. Oncogene. 2003;22:1965-77.
15. Yu D, Wolf JK, Scanlon M, Price JE, Hung MC. Enhanced c-erbB-2/neu expression in human ovarian cancer cells correlates with more severe malignancy that can be suppressed by E1A. Cancer Res. 1993;53:891-8.
16. Eriksson M, Guse K, Bauerschmitz G, Virkkunen P, Tarkkanen M, Tanner M, et al. Oncolytic adenoviruses kill breast cancer initiating CD44+CD24-/low cells. Mol Ther. 2007;15:2088-93.
17. Zhang X, Komaki R, Wang L, Fang B, Chang JY. Treatment of radioresistant stem-like esophageal cancer cells by an apoptotic gene-armed, telomerase-specific oncolytic adenovirus. Clin Cancer Res. 2008;14:2813-23.
18. Kanai R, Rabkin SD, Yip S, Sgubin D, Zaupa CM, Hirose Y, et al. Oncolytic virus-mediated manipulation of DNA damage responses: synergy with chemotherapy in killing glioblastoma stem cells. J Natl Cancer Inst. 2012;104:42-55.
19. Kawashima T, Kagawa S, Kobayashi N, Shirakiya Y, Umeoka T, Teraishi F, et al.

Telomerase-specific replication-selective virotherapy for human cancer. Clin Cancer Res. 2004;10:285-92.
20. Nemunaitis J, Tong AW, Nemunaitis M, Senzer N, Phadke AP, Bedell C, et al. A phase I study of telomerase-specific replication competent oncolytic adenovirus (telomelysin) for various solid tumors. Mol Ther. 2010;18:429-34.
21. Yokozaki H. Molecular characteristics of eight gastric cancer cell lines established in Japan. Pathol Int. 2000;50:767-77.
22. Hashimoto Y, Watanabe Y, Shirakiya Y, Uno F, Kagawa S, Kawamura H, et al. Establishment of biological and pharmacokinetic assays of telomerase-specific replication-selective adenovirus. Cancer Sci. 2008;99:385-90.
23. Sakaue-Sawano A, Kurokawa H, Morimura T, Hanyu A, Hama H, Osawa H, et al. Visualizing spatiotemporal dynamics of multicellular cell-cycle progression. Cell. 2008;132:487-98.
24. Baumann M, Krause M, Hill R. Exploring the role of cancer stem cells in radioresistance. Nat Rev Cancer. 2008;8:545-54.
25. Bao S, Wu Q, McLendon RE, Hao Y, Shi Q, Hjelmeland AB, et al. Glioma stem cells promote radioresistance by preferential activation of the DNA damage response. Nature. 2006;444:756-60.
26. Phillips TM, McBride WH, Pajonk F. The response of CD24(-/low)/CD44+ breast cancer-initiating cells to radiation. J Natl Cancer Inst. 2006;98:1777-85.
27. Nakayama KI, Nakayama K. Ubiquitin ligases: cell-cycle control and cancer. Nat Rev Cancer. 2006;6:369-81.
28. Lee J, Kotliarova S, Kotliarov Y, Li A, Su Q, Donin NM, et al. Tumor stem cells derived from glioblastomas cultured in bFGF and EGF more closely mirror the phenotype and genotype of primary tumors than do serum-cultured cell lines. Cancer Cell. 2006;9:391-403.
29. Ricci-Vitiani L, Lombardi DG, Pilozzi E, Biffoni M, Todaro M, Peschle C, et al. Identification and expansion of human colon-cancer-initiating cells. Nature. 2007;445:111-5.
30. Fujiwara T, Kagawa S, Kishimoto H, Endo Y, Hioki M, Ikeda Y, et al. Enhanced antitumor efficacy of telomerase-selective oncolytic adenoviral agent OBP-401 with docetaxel: preclinical evaluation of chemovirotherapy. Int J Cancer. 2006;119:432-40.
31. Liu D, Kojima T, Ouchi M, Kuroda S, Watanabe Y, Hashimoto Y, et al. Preclinical evaluation of synergistic effect of telomerase-specific oncolytic virotherapy and gemcitabine for human lung cancer. Mol Cancer Ther. 2009;8:980-7.
32. Dean M, Fojo T, Bates S. Tumour stem cells and drug resistance. Nat Rev Cancer. 2005;5:275-84.
33. Ma S, Lee TK, Zheng BJ, Chan KW, Guan XY. CD133+ HCC cancer stem cells confer chemoresistance by preferential expression of the Akt/PKB survival pathway. Oncogene. 2008;27:1749-58.
34. Cheng T, Rodrigues N, Shen H, Yang Y, Dombkowski D, Sykes M, et al. Hematopoietic stem cell quiescence maintained by p21cip1/waf1. Science. 2000;287:1804-8.
35. Liu Y, Elf SE, Miyata Y, Sashida G, Huang G, Di Giandomenico S, et al. p53 regulates hematopoietic stem cell quiescence. Cell Stem Cell. 2009;4:37-48.
36. Sutterluty H, Chatelain E, Marti A, Wirbelauer C, Senften M, Muller U, et al. p45SKP2 promotes p27Kip1 degradation and induces S phase in quiescent cells. Nat Cell Biol. 1999;1:207-14.

37. Kamura T, Hara T, Matsumoto M, Ishida N, Okumura F, Hatakeyama S, et al. Cytoplasmic ubiquitin ligase KPC regulates proteolysis of p27(Kip1) at G1 phase. Nat Cell Biol. 2004;6:1229-35.
38. Lomazzi M, Moroni MC, Jensen MR, Frittoli E, Helin K. Suppression of the p53- or pRB-mediated G1 checkpoint is required for E2F-induced S-phase entry. Nat Genet. 2002;31:190-4.
39. Steegenga WT, van Laar T, Riteco N, Mandarino A, Shvarts A, van der Eb AJ, et al. Adenovirus E1A proteins inhibit activation of transcription by p53. Mol Cell Biol. 1996;16:2101-9.

## Figure Legends

**Fig. 1 CD133$^+$ cancer stem-like cells in human gastric cancer exhibit CS-like cell properties and are more quiescent.**

**A,** Flow cytometric analysis of CD133 expression in parental (P) and radioresistant (R) MKN45 cells. Representative dot plots (left) and data from five experiments (right) are shown. **B,** CD133$^+$ MKN45 cancer cells exhibit CS-like properties. Representative image of colonies from CD133$^+$ or CD133$^-$ cells. Histogram shows the size of colonies from CD133$^+$ or CD133$^-$ cells (left). Quantitative measurement of the tumor sphere-forming potential of CD133$^+$ and CD133$^-$ cells (middle). Representative image of tumor spheres derived from CD133$^+$ and CD133$^-$ cells. Histogram shows the numbers of tumor spheres from CD133$^+$ or CD133$^-$ cells. Scale bars, 500 μm. Tumorigenicities of CD133$^+$ and CD133$^-$ cells in immunodeficient NOD/SCID mice (right). Growth curve of each tumors and representative photograph are shown. **C,** Cell viability of CD133$^+$ and CD133$^-$ cells from radioresistant MKN45 cells to 5-fluorouracil, cisplatin, paclitaxel and irradiation. **D,** Time-lapse imaging of CD133$^+$ and CD133$^-$ cells from radioresistant MKN45 cells expressing cell cycle-dependent fluorescent proteins (FUCCI) (upper). The cells in $G_0$/ $G_1$, S, or $G_2$/M phases appear red, yellow, or green, respectively. Histogram shows the cell cycle phase of FUCCI-expressing CD133$^+$ and CD133$^-$ cells cultured for 48 hours after sorting (lower right). The percentage of cells in $G_0$/ $G_1$, S, and $G_2$/M phases are shown. Cell proliferation rate of CD133$^+$ and CD133$^-$ cells (lower left). Scale bars, 50 μm. Data are shown as means ± SD (n = 5). $^*P < 0.01$.

**Fig. 2 OBP-301 lethally induces S phase transition of quiescent CD133$^+$ cancer stem-like cells with decreasing CS-like cell frequency via enhanced viral replication.**

**A,** OBP-301 efficiently kills CD133$^+$ CS-like cells. Cell viability of CD133$^+$ and CD133$^-$ cells from MKN45 cells to OBP-301 infection. (left). The percentages of CD133$^+$ cells in radioresistant MKN45 cells treated with OBP-301, cisplatin, or radiation were analyzed by flow cytometry (right). **B,** OBP-301 can replicate more in CD133$^+$ that have more activity of hTERT than in CD133$^-$ cells. Expression of *hTERT* mRNA in CD133$^+$ and CD133$^-$ MKN45 cells assessed by quantitative real-time RT-PCR (qRT-PCR) (upper left). The relative levels of *hTERT* mRNA were calculated after normalization with reference to the expression of *PBGD* mRNA. Expression of *E1A* mRNA in CD133$^+$ and CD133$^-$MKN45 cells after OBP-301 infection at an MOI of 10 PFU/cell for 2 hours. Expression of *E1A* mRNA was analyzed over the following 3 days qRT-PCR (upper middle). The relative levels of *E1A* mRNA were calculated after normalization with reference to the expression of *GAPDH* mRNA. Western blot analysis of E1A expression in CD133$^+$ and CD133$^-$ MKN45 cells treated with OBP-301 for 48 hours (lower left). Quantitatively relative expression level of E1A protein, normalized to b-actin, using NIH ImageJ software (lower left). Quantitative measurement of viral DNA replication in CD133$^+$ and CD133$^-$ MKN45 cells after OBP-301 infection at an MOI of 10 PFU/cell for 2 hours (lower right). *E1A* copy number was analyzed over the following 3 days using qPCR. **C,** Time-lapse imaging of FUCCI-expressing CD133$^+$ and CD133$^-$ cells treated with OBP-301 at an MOI of 20 PFU/cell. The cells in $G_0$/ $G_1$, S, or $G_2$/M phases appear red, yellow, or green, respectively. Histogram shows the cell cycle phases of FUCCI-expressing CD133$^+$ and CD133$^-$ cells treated with OBP-301 for 48 hours. The percentage of cells in $G_0$/ $G_1$, S, and $G_2$/M phases are shown. **D,** Western blot analysis of E2F1, c-Myc, phospho-Akt, Akt, p53, p21 and p27 expression in CD133$^+$ cells treated with OBP-301, cisplatin, or radiation for 48 hours. β-actin was assayed as a loading control for all experiments. Data are shown as means ± SD (n = 5). **P* < 0.05, ***P* < 0.01.

**Fig. 3 Three-dimensional tumor spheres maintain CD133$^+$ cells by arresting the cell cycle.**

**A,** Time-lapse images of FUCCI-expressing CD133$^+$ cells in three-dimensional culture without serum. Purified FUCCI-expressing CD133$^+$ cells were cultured on agar in serum-free medium containing EGF and bFGF for 48 hours (upper). The cells in $G_0$/ $G_1$, S, or $G_2$/M phases appear red, yellow, or green, respectively. Histogram shows the cell cycle phase of FUCCI-expressing CD133$^+$ cells in three-dimensional culture without serum (lower). The percentage of cells in $G_0$/ $G_1$, S, and $G_2$/M phases are shown. **B,** Representative image of tumor spheres from FUCCI-expressing CD133$^+$ and CD133$^-$ cells (upper). Histogram shows the cell cycle phase of tumor spheres from FUCCI-expressing CD133$^+$ and CD133$^-$ cells (lower). **C,** Time-lapse images of FUCCI-expressing CD133$^+$ cells in monolayer culture or FUCCI-expressing tumor spheres in three-dimensional culture without serum (3D without serum) or tumor spheres in monolayer culture with serum (monolayer culture) (upper). Histogram shows the cell cycle phase of FUCCI-expressing CD133$^+$ cells in 2D culture, FUCCI-expressing established tumor spheres in 3D without serum, or tumor sphere in monolayer culture with serum (monolayer culture) (lower). **D,** Comparison of changes in CD133$^+$ positive ratio of CD133$^+$ cells in monolayer culture, tumor spheres in 3D culture without serum, or with serum. Representative dot plots (left) and data from three experiments (right) are shown. Data are shown as means ± SD (n = 5). **P* < 0.01. Scale bars, 500 μm.

**Fig. 4 Visualization of eliminating dormant tumor spheres by virus infection.**

**A,** Time-lapse images of tumor spheres treated with OBP-301 ($5 \times 10^6$ PFU), cisplatin (10 μM), or radiation (10 Gy). The cells in $G_0$/ $G_1$, S, or $G_2$/M phases appear red, yellow, or green, respectively. **B,** Histogram shows the cell cycle phase of the spheres with OBP-301, cisplatin, or radiation. The percentage of cells in $G_0$/ $G_1$, S, and $G_2$/M phases are shown. **C,** Representative image of control, OBP-301, cisplatin, or radiation treated spheres (upper). Histogram shows that relative cell viability of treated tumor spheres (lower). **D,** The $CD133^+$ tumor spheres treated as above were stained for E2F1, phospho-Akt, p53, and p21. Immuofluorescent staining was visualized by confocal laser microscopy. Scale bars, 100 µm. Data are shown as means ± SD (n = 5). **P* < 0.01.

**Fig. 5 OBP-301 induces cell-cycle progression and efficiently kills dormant cancer cells resistant to conventional therapy in established human tumor xenografts.**

$CD133^+$ rich radioresistant MKN45 cells ($5 \times 10^6$ cells/mouse) were injected subcutaneously into the left flanks of mice. When the tumors reached approximate 6 mm in diameter (tumor volume, 100-120 $mm^3$), mice were administered OBP-301 intratumorally ($1 \times 10^8$ PFU/tumor), injected intraperitoneally with cisplatin (4mg/kg), or exposed to 2Gy of radiation for three cycles every 3 days. **A,** The growth curves of tumors derived from radioresistant MKN45 cells after treatment with OBP-301, cisplatin or radiation. Black arrows indicate the day of treatment. **B,** Expression of *CD133* mRNA in tumors treated with OBP-301, cisplatin or radiation at 1, 2 and 3 weeks after treatment (upper). Representative image of CD133-stained tumor section treated with OBP-301, cisplatin, or radiation (lower left). Scale bars, 100 µm. Histogram shows the percentages of $CD133^+$ cells *in vivo* tumor treated with OBP-301, cisplatin, or radiation (lower right). The percentage of $CD133^+$ cells were calculated by dividing the number of $CD133^+$ cells by the total number of cells. Data are shown as means ± SD (n = 3). **P* < 0.05. **C, D,** FUCCI-expressing MKN45 cells ($5 \times 10^6$ cells/mouse) were injected subcutaneously into the left flanks of mice. When the tumors reached approximately approximate 7 mm in diameter (tumor volume, 150-180 $mm^3$), mice were administered OBP-301 intratumorally ($1 \times 10^8$ PFU/tumor), injected intraperitoneally with cisplatin (4mg/kg) or paclitaxel (5mg/kg) for three cycles every 3 days. Representative images of cross-sections of FUCCI-expressing MKN45 subcutaneous tumor of control, OBP-301, cisplatin, or paclitaxel treated mice (left). The cells in $G_0$/ $G_1$, S, or $G_2$/M phases appear red, yellow, or green, respectively. Histogram shows the cell cycle phase of FUCCI-expressing MKN45 subcutaneous tumor from control, OBP-301, cisplatin, or paclitaxel treated mice (right). The percentage of cells in $G_0$/ $G_1$, S, and $G_2$/M phases are shown. Data are shown as means ± SD (n = 5). **P* < 0.05. Scale bars, 500μm.

**Fig. 6 OBP-301 sensitizes quiescent CD133$^+$ CS-like cells to chemotherapy by inducing cell-cycle progression.**

**A,** Representative image of tumor spheres from FUCCI-expressing CD133$^+$ cells after treatment with cisplatin, paclitaxel, OBP-301 and the combination of OBP-301 and chemotherapy (upper). The cells in $G_0$/ $G_1$, S, or $G_2$/M phases appear red, yellow, or green, respectively. The area of tumor sphere was calculated using NIH ImageJ software (lower). Data are shown as means ± SD (n = 5). **P* < 0.05. Scale bars, 500 μm. **B,** Histogram shows the cell cycle phase of tumor spheres from FUCCI-expressing CD133$^+$ cells after treatment with chemotherapy, OBP-301 and the combination of OBP-301 and chemotherapy. The percentage of cells in $G_0$/ $G_1$, S, and $G_2$/M phases are shown. Data are shown as means ± SD (n = 5). **P* < 0.05. **C,** FUCCI-expressing MKN45 cells ($5 \times 10^6$ cells/mouse) were injected subcutaneously into the left flanks of mice. When the tumors reached approximately about 8 mm in diameter (tumor volume, 300 $mm^3$), mice were administered OBP-301 intratumorally ($1 \times 10^8$ PFU/tumor), injected intraperitoneally with cisplatin (4mg/kg) or paclitaxel

(5mg/kg) for five cycles every 3 days. The growth curves of tumors derived from FUCCI-expressing MKN45 cells after treatment with chemotherapy, OBP-301 or the combination of OBP-301 and chemotherapy (left). Red and green arrows indicate the day of treatment with OBP-301 and chemotherapy, respectively. Macroscopic photographs of FUCCI-expressing tumors of control, treated with OBP-301, cisplatin, paclitaxel or the combination of OBP-301 and chemotherapy (right). Scale bars, 10 mm. **D,** Representative image of cross-sections of FUCCI-expressing MKN45 subcutaneous tumor of control, OBP-301, cisplatin, paclitaxel or the combination of OBP-301 and chemotherapy treated mice (upper). Histogram shows cell cycle phase of FUCCI-expressing MKN45 subcutaneous tumor of control, treated with OBP-301, cisplatin, paclitaxel or the combination of OBP-301 and chemotherapy (lower). Data are shown as means ± SD (n = 6). **P* < 0.05, ANOVA. Scale bars, 500μm.

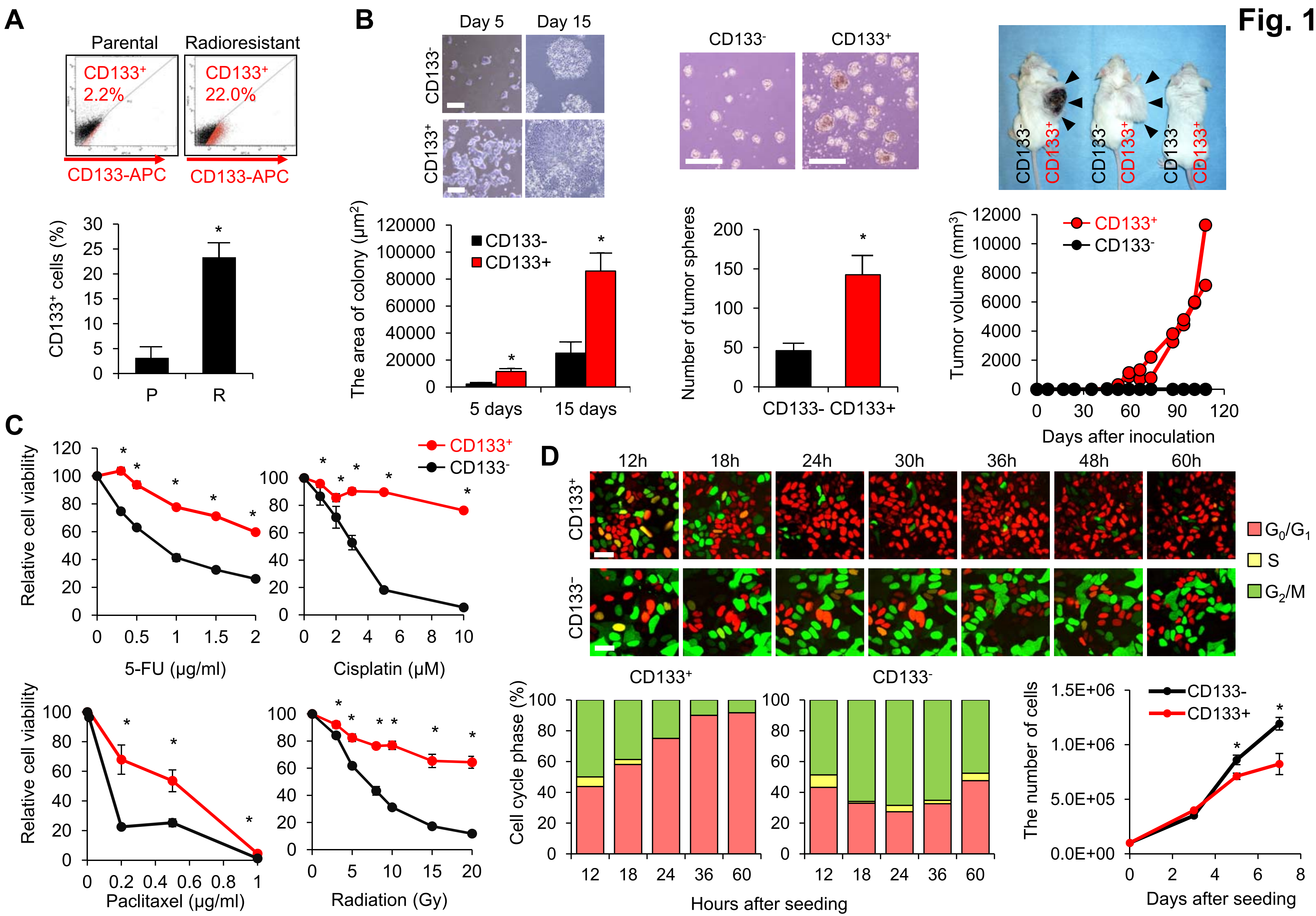
Fig. 1
A
Parental
Radioresistant
CD133+ 2.2%
CD133+ 22.0%
CD133-APC
CD133+ cells (%)
P
R
B
Day 5
Day 15
CD133-
CD133+
The area of colony (μm2)
5 days
15 days
Number of tumor spheres
CD133- CD133+
Tumor volume (mm3)
Days after inoculation
C
Relative cell viability
5-FU (μg/ml)
Cisplatin (μM)
Paclitaxel (μg/ml)
Radiation (Gy)
D
12h
18h
24h
30h
36h
48h
60h
G0/G1
S
G2/M
Cell cycle phase (%)
Hours after seeding
The number of cells
Days after seeding

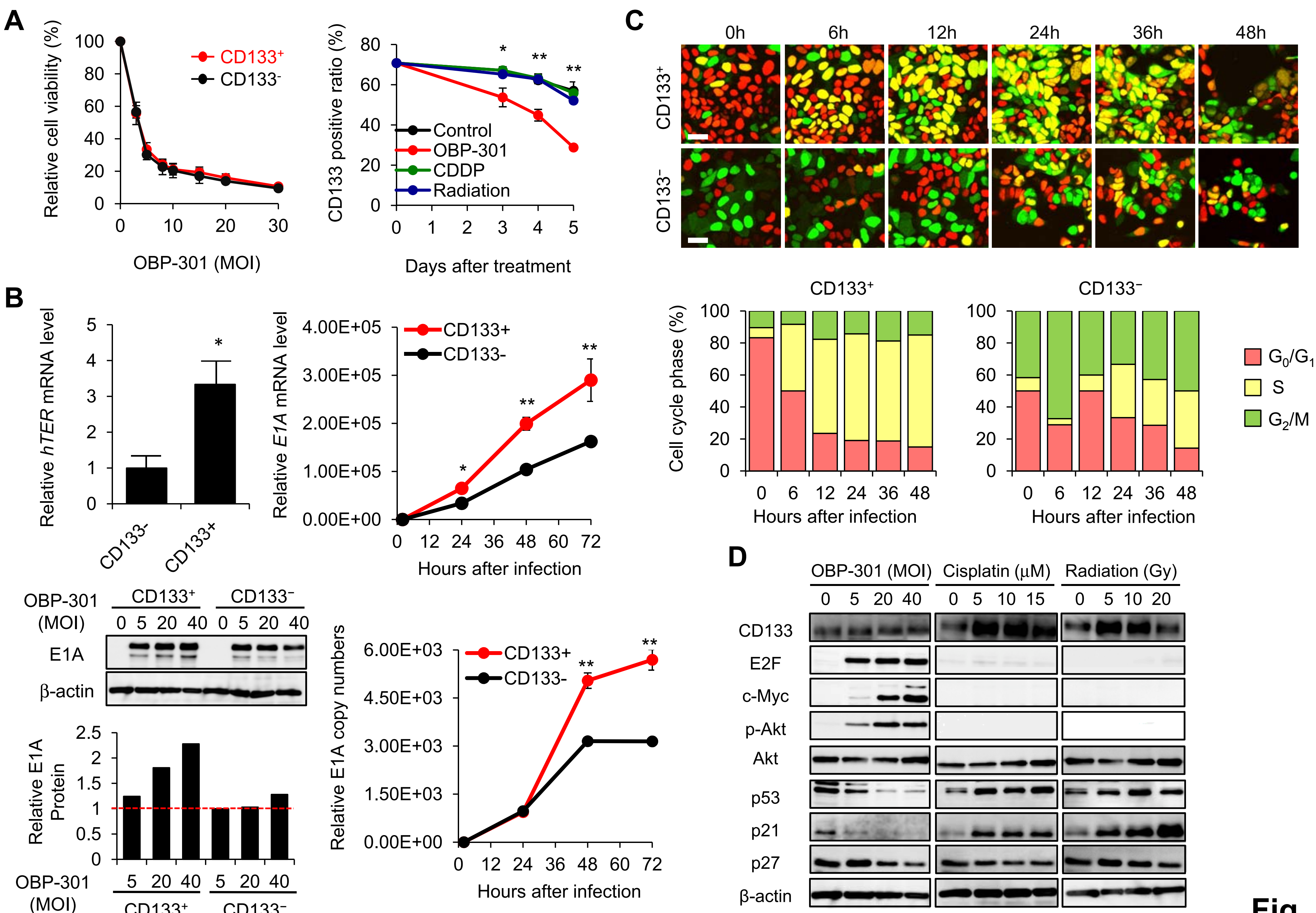

A
Relative cell viability (%)
OBP-301 (MOI)
CD133+
CD133-
CD133 positive ratio (%)
Days after treatment
Control
OBP-301
CDDP
Radiation
B
Relative hTER mRNA level
CD133-
CD133+
Relative E1A mRNA level
Hours after infection
OBP-301 (MOI)
E1A
β-actin
Relative E1A Protein
Relative E1A copy numbers
C
0h
6h
12h
24h
36h
48h
Cell cycle phase (%)
Hours after infection
G0/G1
S
G2/M
D
OBP-301 (MOI)
Cisplatin (μM)
Radiation (Gy)
CD133
E2F
c-Myc
p-Akt
Akt
p53
p21
p27
β-actin


Fig. 2

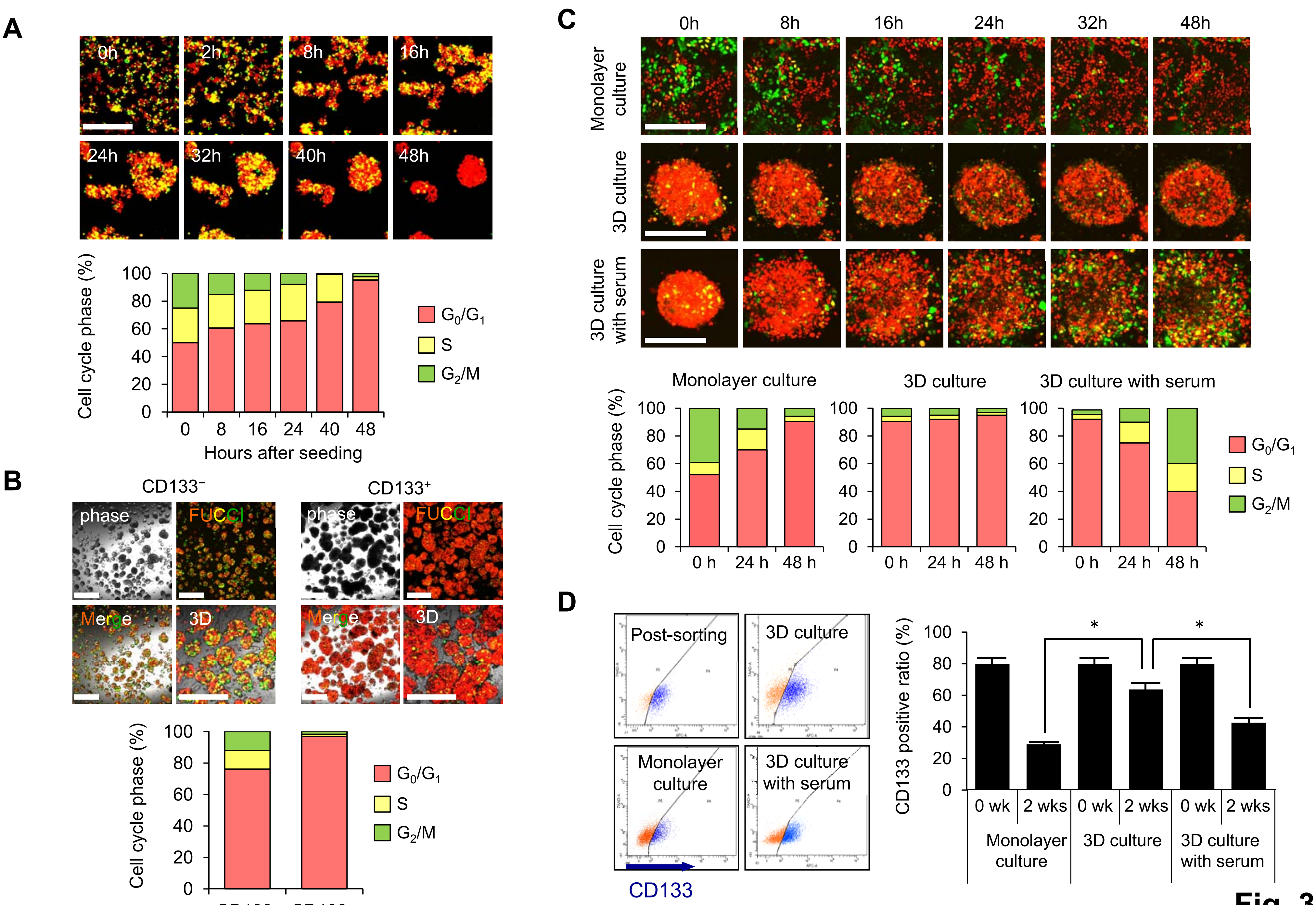
A
0h
2h
8h
16h
24h
32h
40h
48h
Cell cycle phase (%)
Hours after seeding
G0/G1
S
G2/M
B
CD133⁻
CD133⁺
phase
FUCCI
Merge
3D
CD133-
CD133+
C
Monolayer culture
3D culture
3D culture with serum
0 h
24 h
48 h
D
Post-sorting
3D culture
Monolayer culture
3D culture with serum
CD133
CD133 positive ratio (%)
0 wk
2 wks
*

Fig. 3

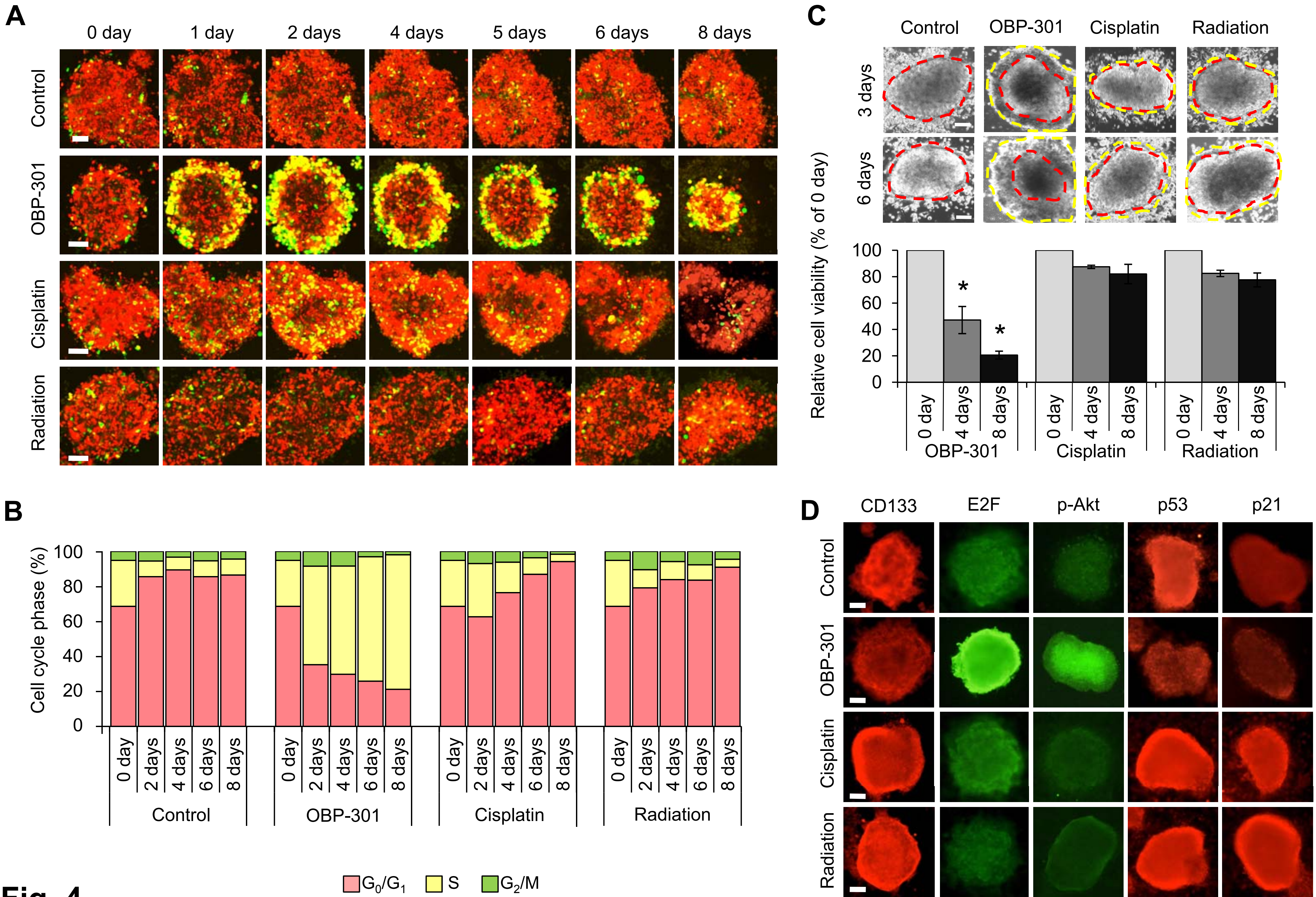
A
0 day
1 day
2 days
4 days
5 days
6 days
8 days
Control
OBP-301
Cisplatin
Radiation
B
Cell cycle phase (%)
0
20
40
60
80
100
0 day
2 days
4 days
6 days
8 days
Control
OBP-301
Cisplatin
Radiation
$G_0/G_1$
S
$G_2/M$
C
Control
OBP-301
Cisplatin
Radiation
3 days
6 days
Relative cell viability (% of 0 day)
0
20
40
60
80
100
*
*
0 day
4 days
8 days
OBP-301
Cisplatin
Radiation
D
CD133
E2F
p-Akt
p53
p21
Control
OBP-301
Cisplatin
Radiation

**Fig. 4**

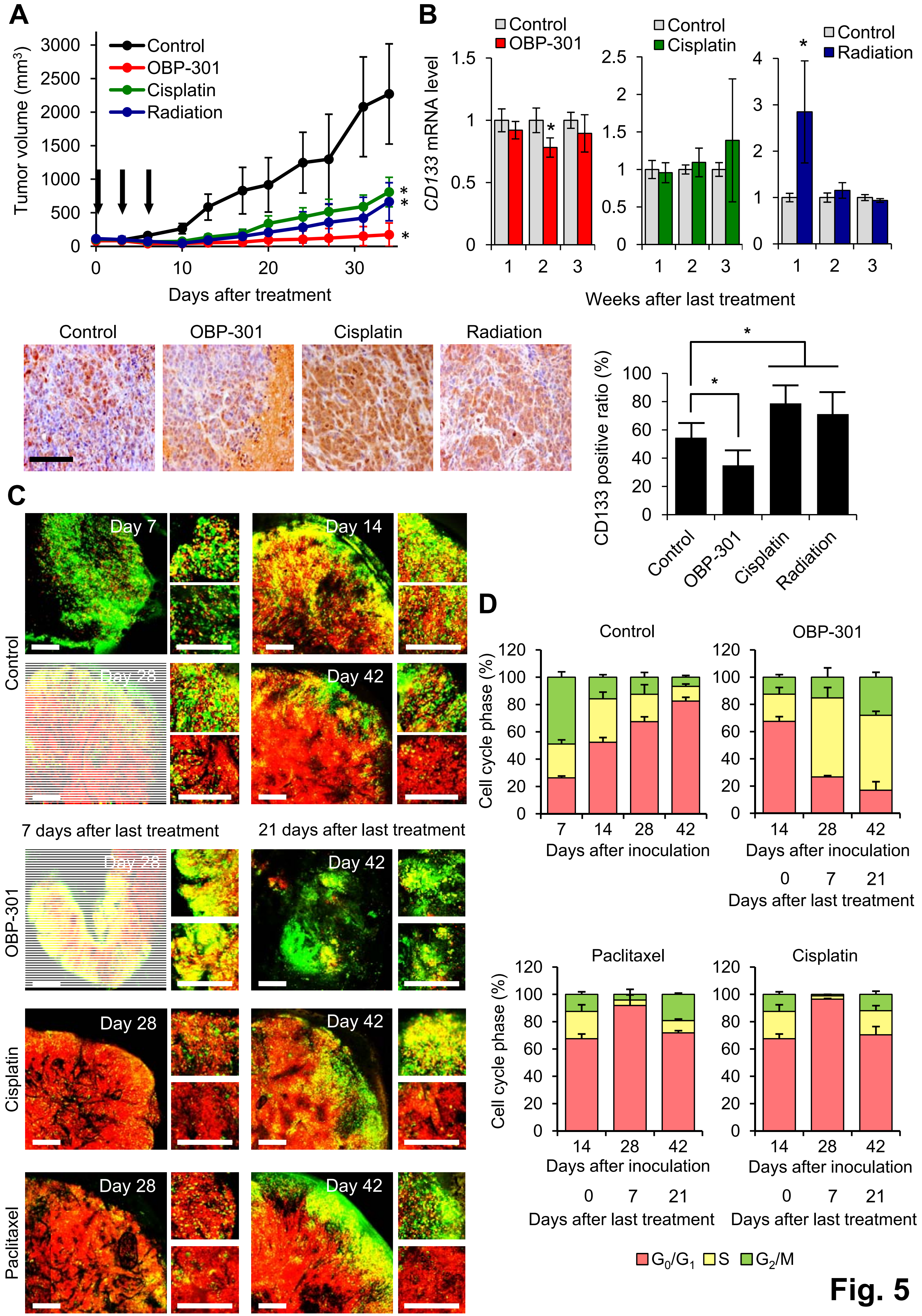

A
Control
OBP-301
Cisplatin
Radiation
Tumor volume (mm³)
Days after treatment
B
CD133 mRNA level
Weeks after last treatment
Control
OBP-301
Cisplatin
Radiation
CD133 positive ratio (%)
C
Day 7
Day 14
Day 28
Day 42
Control
OBP-301
Cisplatin
Paclitaxel
7 days after last treatment
21 days after last treatment
D
Cell cycle phase (%)
Days after inoculation
Days after last treatment
Paclitaxel
G0/G1
S
G2/M


Fig. 5

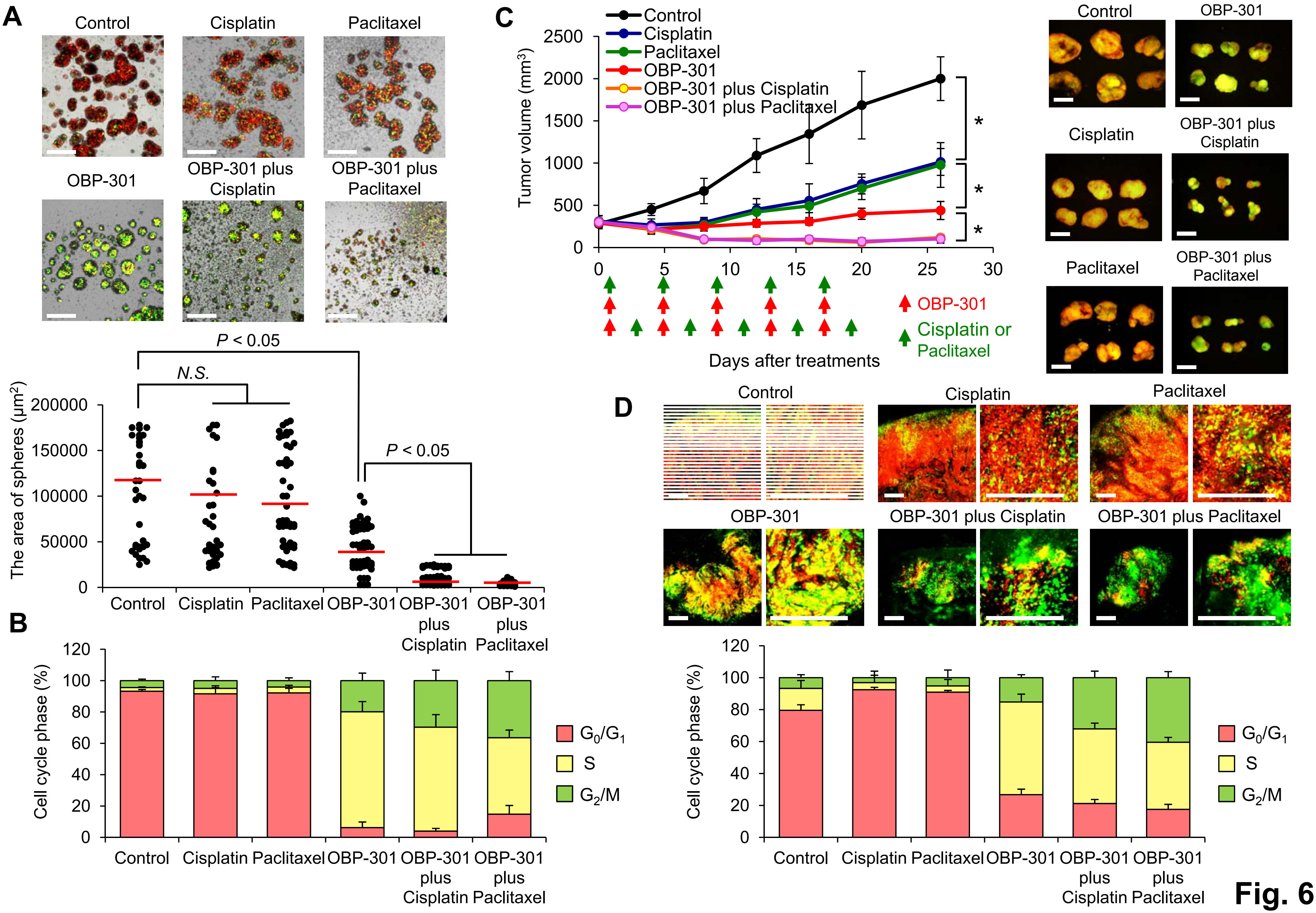
A
Control
Cisplatin
Paclitaxel
OBP-301
OBP-301 plus Cisplatin
OBP-301 plus Paclitaxel
P < 0.05
N.S.
P < 0.05
The area of spheres (μm²)
200000
150000
100000
50000
0
Control
Cisplatin
Paclitaxel
OBP-301
OBP-301 plus Cisplatin
OBP-301 plus Paclitaxel
B
Cell cycle phase (%)
120
100
80
60
40
20
0
G0/G1
S
G2/M
C
Control
Cisplatin
Paclitaxel
OBP-301
OBP-301 plus Cisplatin
OBP-301 plus Paclitaxel
Tumor volume (mm³)
2500
2000
1500
1000
500
0
0
5
10
15
20
25
30
*
*
*
OBP-301
Cisplatin or Paclitaxel
Days after treatments
D
Control
Cisplatin
Paclitaxel
OBP-301
OBP-301 plus Cisplatin
OBP-301 plus Paclitaxel
Fig. 6